PCCP

PAPER

View Article Online
View Journal | View Issue

Cite this: *Phys. Chem. Chem. Phys.*, 2017, **19**, 31499

Molecular mechanism of activation of *Burkholderia cepacia* lipase at aqueous–organic interfaces

Ivan Pires de Oliveira, Gabriel Ernesto Jara and Leandro Martínez *

Received 3rd July 2017,
Accepted 11th November 2017

DOI: 10.1039/c7cp04466f

rsc.li/pccp

Lipases are water-soluble enzymes that catalyze the hydrolysis of lipids. Since lipids are mostly hydrophobic, lipase activity occurs preferentially at interfaces of aqueous and organic phases. In this work, we study the molecular mechanisms by which the *Burkholderia cepacia* lipase (BCL) is activated at interfaces of water with octane and with methyl caprylate (CAME). We show that BCL assumes very rapidly a preferential orientation at the interfaces, in which the active site is exposed to the organic phase. With BCL oriented to the interface, we compute the free energy of the aperture of the catalytic pocket using Adaptive Biasing Force MD simulations. The exposure to the organic phase promotes a clear stabilization of the open form of the catalytic pocket relative to the enzyme in water. This stabilization stems from the hydrophobicity of domains U1 and U2, which allows the penetration of organic solvents into the catalytic cleft impeding the closure of the pocket. Our results suggest that the structure and hydrophobicity of BCL are optimized for its activation in biphasic systems through the regulation of the accessibility of the catalytic pocket by, and for, hydrophobic substrates. The understanding of this mechanism may be useful for the design of proteins with targeted activation.

1 Introduction

Enzymes have evolved to facilitate reactions in a variety of molecular environments, some of them being useful for technological or biomedical applications.[1] Lipases, in particular, are enzymes that catalyze the hydrolysis of lipids and, therefore, must be able to transition between aqueous and hydrophobic environments to approach the substrates.[2] Because of this, it was found that lipases can assume different conformations, catalyze different reactions, and be solvated by complex microheterogeneous environments in mixtures of aqueous and hydrophobic solvents.[3–6]

Triacylglycerol lipases (EC 3.1.13) promote the catalysis of triacylglycerols (TAGs) into free fatty acids.[7,8] Therefore, they convert mostly hydrophobic substrates into amphiphilic products, using water as a substrate for the hydrolysis.[2,8] It is believed that the activity of these enzymes involves their diffusion from the aqueous phase to the interface between the aqueous and organic phases, as shown in Fig. 1. Specifically, the organic phase might be a saturated solution of the apolar substrate, the substrate dissolved in an organic solvent, or a liquid phase of the pure lipid.[8,9] When reaching the interface, the enzyme (E) must achieve an active conformation (E*), and bind the substrate (S) which is found mostly in the hydrophobic phase, leading to the formation of the catalytic complex (E*S). Once the chemical reaction takes place, the products should be released to the aqueous solution, where they can be available for other cellular processes or extracted for technological applications.[10,11]

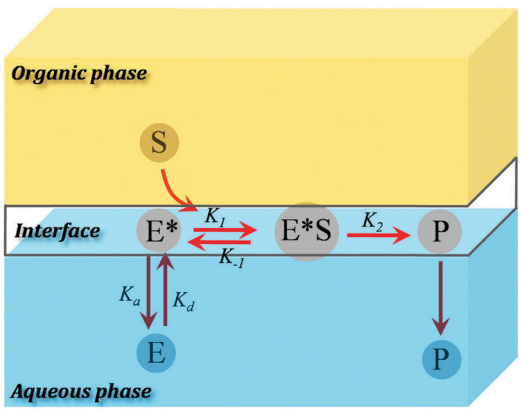

Fig. 1 Kinetic model of activation of lipases in interfaces, as proposed by Desnuelle and co-workers.[12] The enzyme (E) must migrate to the interface, where it assumes a conformation (E*) which facilitates substrate binding and formation of the enzyme–substrate complex (E*S). The chemical reaction then takes place and the products are released to the aqueous phase.[8,12]

Institute of Chemistry and Center for Computational Engineering & Science, University of Campinas, Campinas, SP, Brazil. E-mail: leandro@iqm.unicamp.br

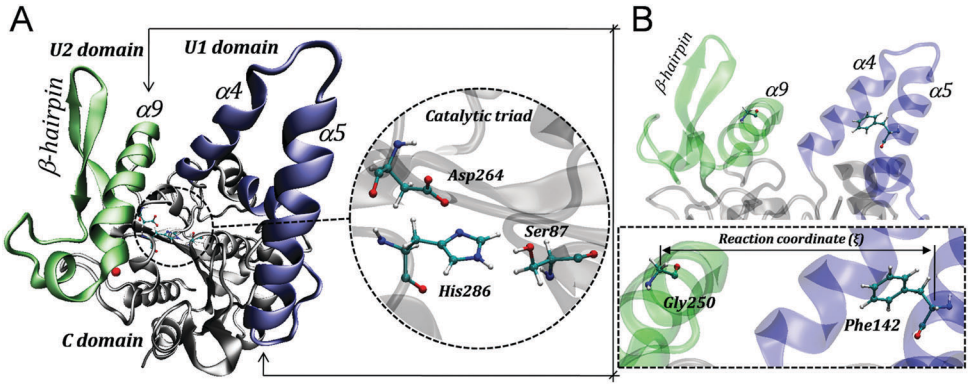

Fig. 2 Three-dimensional structure of the BCL enzyme. (A) Overall structure and detailed view of the catalytic triad residues (Ser87, Asp264, and His286). The calcium ion is represented by a red sphere. (B) The distance between helices 5 and 9 defines a reaction coordinate associated with the opening and closure of the catalytic pocket. In our computations, we used the distance between the α-carbons of Gly250 (from helix 9) and Phe142 (from helix 5) to represent the reaction coordinate.

The *Burkholderia cepacia* lipase (BCL) is a triacylglycerol lipase which should display a mechanism similar to that of general lipases, as represented in Fig. 1. Thus, it might migrate to the aqueous/organic interface and assume a conformation which facilitates the association of the substrates. BCL has three domains, as shown in Fig. 2: U1 (residues 118–166), U2 (residues 215–261) and C (1–117; 167–214; 262–320). The U1 and U2 domains are associated with the exposure of the catalytic site.[13,14] Some studies supported the possibility that BCL has two clearly distinct conformations: (1) with helices α5 and α9 distant from each other, characterizing an ''open'' state; (2) with helix α5 folded over helix α9, defining a ''closed'' state. Fluctuations between these two conformations are associated with the exposure of the catalytic residues to the solvent, and can be spontaneously observed in classical molecular dynamics in homogeneous solvents in the sub-microsecond time-scale for BCL[15–18] and other lipases.[19]

Other lipases display mechanisms of activation similar to that of BCL, in the sense of being dependent on the polarity of the environment. For instance, the activation was observed to occur independently of the concentration of the substrates in interfaces of water and toluene for the lipases of *Candida rugosa*, *Rhizomucor mihei*, and *Thermomyces lanuginosa*.[3] The aperture of the binding pocket is, therefore, dependent on the hydrophobic solvation of specific domains, not requiring induction by the substrate.

Here, we obtain a molecular picture of the complete mechanism of activation of the BCL enzyme in aqueous/organic interfaces through molecular dynamics simulations. We show that (1) the enzyme goes through a rapid orientation at the interfaces; (2) the orientation of the enzyme at the interface results in the exposure of the catalytic pocket, in a process that is thermodynamically favored and induced by the interactions of specific protein domains with the organic phase. The activation of the enzyme by its interaction with the interface is quantified relative to the enzyme in water by computing the free energy profiles along the coordinate of the aperture of the catalytic pocket. We show that the interactions of the hydrophobic U1 and U2 domains with the organic phase, and the penetration of organic substrates into the catalytic pocket favor thermodynamically the open, active, conformation of the enzyme. The mechanisms of activation described here might be extrapolated for other lipases with similar interfacial function and activation.[20]

2 Materials and methods

2.1 Conventional molecular dynamics simulations

The crystal structure of BCL (PDB ID: 1YS1) was used for all simulations. It has a resolution of 1.10 Å, 320 residues, one calcium ion and a ligand (hexylphosphonic acid (*R*)-2-methyl-3-phenylpropyl ester) bound.[14] The ligand was removed. The protein was solvated using Packmol[21,22] at the interfaces of water and octane or CAME (caprylic acid methyl ester). Random initial orientations of the protein relative to the interfaces were used. A third system was built using only water as a solvent. Sodium and chloride ions were added to neutralize the system and mimic approximate physiological ionic strengths. Details of the systems simulated are presented in Table 1. Octane and CAME were chosen as the organic phases to represent the polarity of organic fatty acids and fats which are commonly used in lipase-catalyzed processes.[23] We chose to simulate relatively small organic chains to avoid problems with the relaxation of the structure of the solvents.

All the simulations were performed with NAMD[24] and the figures were produced using VMD.[25] We used isothermal–isobaric (*NPT*) conditions at 298.15 K and 1 atm. A Langevin barostat was used with a period of 200 ps and a decay time of 100 ps to control the pressure. Temperature was controlled using Langevin dynamics with a perturbation frequency of 10 ps^{-1}. The CHARMM36 force-field was used for the protein and the ions.[26,27] The TIP3P model was used for water.[28] The octane and caprylic acid methyl ester parametrizations were performed with the CGenFF platform.[29,30]

Conventional MD simulations were performed as follows: (1) keeping all the protein atoms fixed in space, 15 000 steps of

Table 1 Compositions of the systems simulated. Four independent 400 ns simulations starting with different orientations of the protein at the interface were performed for each system

			Number of molecules		
System	Notation	ABF simulation	Water	CAME	Octane
1	CAME	No	15 000	2000	0
2	OCTA	No	15 800	0	2500
3	Water	Yes	20 800	0	0
4	CAME	Yes	15 000	2000	0
5	OCTA	Yes	15 800	0	2500

Conjugate-Gradient (CG) energy minimization were performed, followed by 2 ns of constant-temperature constant-volume (*NVT*) simulations at 298.15 K, to allow solvent relaxation. (2) Fixing only the Cα protein atoms, the energy of the system was minimized by 500 CG steps, and relaxed by 2 ns of MD simulation with isothermic-isobaric conditions (*NPT*) at 298.15 K and 1 bar. (3) All the constraints were removed, and 4 independent production simulations of 400 ns were performed to probe the reorientation of the protein structure at the interface, for each solvent.

The orientation of the protein relative to the interface was defined by computing the scalar angle between the normal vectors to the organic phases and to the active cleft. The normal vector to the active cleft was defined from the centers of mass of the residues 117–125, 134–151, and 246–258 (helices α4, α5 and α9) and residues 81–87. Only backbone atoms were considered. The normal vectors to the organic phases were computed from the centers of the masses of the two phases. A schematic representation of the vectors is shown in Fig. 3.

2.2 Free energy profiles

To obtain the free energy profiles of the aperture and closure of the catalytic pocket, we used the Adaptive Biasing Force (ABF) method, as implemented in NAMD.[31–33]

The ABF method aims at the application of an external force to the simulation that exactly counteracts the average force the system experiences along the reaction coordinate of interest. The average force is estimated from the simulation itself, and the estimate is continuously improved for every point along the reaction coordinate whenever the system passes at that coordinate. When the average force is precisely estimated along the complete reaction coordinate and the opposite force is applied, the dynamics along that coordinate becomes diffusive, allowing the system to sample conformations that would not be sampled in a conventional simulation. Additionally, since the average force is the gradient of the free energy, the potential of

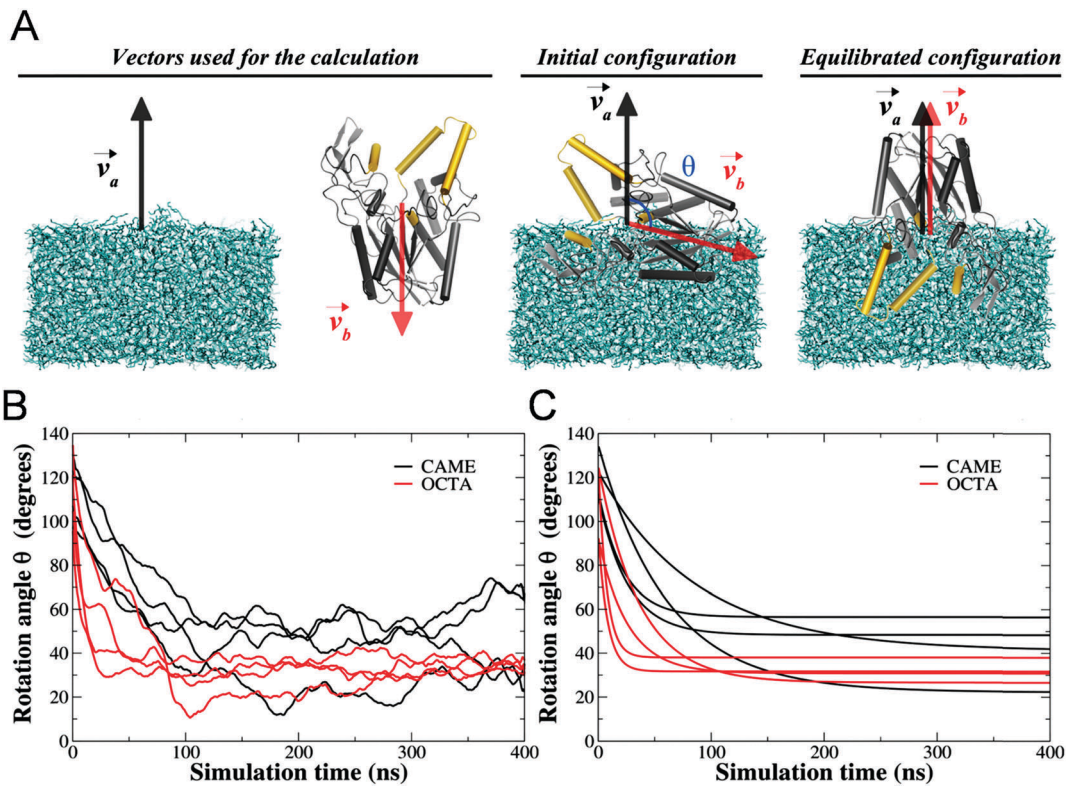

Fig. 3 Rotation of the BCL enzyme at the interfaces of water with octane and CAME. (A) The rotation angle is defined as the angle between a vector normal to the interface and pointing to the aqueous phase (gray), and a vector (red) centered at the active-site cleft (yellow). With these definitions, the initial configuration displays these vectors roughly orthogonal to each other. Their colinearity indicates that the active-site cleft is oriented toward the organic phase. (B) Time-dependence of the rotation angle. (C) Exponential fits to the time dependence of the rotation angle. The characteristic rotation times vary between 7 and 36 ns^{-1} in octane and between 22 and 86 ns^{-1} in CAME, indicating that the polarity of the organic phase is associated with the rate of reorientation.

mean force (the free energy along the reaction coordinate) can be obtained from the average force by simple integration.[31,33]

The reaction coordinate to represent the aperture of the binding pocket was defined as the distance between the Cα atoms of residues Phe142 from helix 5, and Gly250 from helix 9 (See Fig. 2). This reaction coordinate was used because it was identified in previous works as adequate for the representation of the opening of the catalytic cleft.[15,16] The distance between these residues was sampled in the 5.0 Å to 30.0 Å interval with bins of 0.1 Å. A force constant of 10.0 kcal mol^{-1} $Å^{-2}$ was used at the reaction coordinate boundaries. A minimum sampling of 5000 simulation steps at each bin was used to estimate the average force, before the application of the ABF force. Three independent 200 ns of simulation of each system were performed to obtain converged free energy profiles. In Fig. 9, we express the mean and standard deviations of the three simulations.

Finally, structural analyses such as the radius of gyration, root mean square deviation (RMSD), and atomic distances were performed with the tools available in the MDAnalysis suite[34] and VMD packages.[25] Fig. 7C, which illustrates the fluctuations of the most and least mobile regions of the protein, was produced using the MDLovoFit package.[35]

3 Results and discussion

3.1 Orientation of BCL at the interfaces

Our simulations started with the protein randomly oriented at the interfaces of the water and organic phases. We aimed at the description of the functional orientation of the enzyme at the interface without introducing any bias. Perhaps surprisingly fast, the BCL enzyme rotated in such a way to expose the catalytic cleft to the organic phase in all simulations. These rotations were always complete in less than 150 ns of simulation, as shown in Fig. 3, with the characteristic reorientational times varying from 7 to 36 ns^{-1} at the interface with octane, and from 22 to 86 ns^{-1} at the interface with CAME. Therefore, the reorientation at the less polar interface is generally faster (Fig. 3B and C). The initial orientation of the enzyme, using the vectors chosen in this study (Fig. 3A), varied between 100° and 150°. The orientation of the enzyme at the octane interface appears to be more stable, and converged systematically to a rotation angle of ∼35°. At the interface with CAME, the final orientation of the enzyme was more variable, with angles ranging between ∼20° and 55°.

The U1 and U2 domains assume approximately parallel orientations to the interface, but the immersion in the organic phase is different in each case. Domains U1 and U2 are more hydrophobic, and domain C is more hydrophilic, and these differences in hydrophilicity determine the final orientation of the enzyme at the interface for each solvent. CAME is much more miscible with water than octane due to the polarity of its methyl ester group, as shown in Fig. 4, thus it can interact favorably with the C domain. Also, the interactions of CAME with polar side chains and backbone groups of BCL retard its rotation. These interactions are not present in octane, resulting in the different equilibrium orientations of BCL.

The exposure of the catalytic triad to the organic phase is represented in Fig. 5. The rotation of BCL leads to a stable orientation at the interface that is highly suggestive of an activated state. Because of the higher polarity of CAME relative to octane, the protein is partially immersed in the organic phase of CAME, while its interactions with octane are only superficial. In both cases, however, the molecules of the

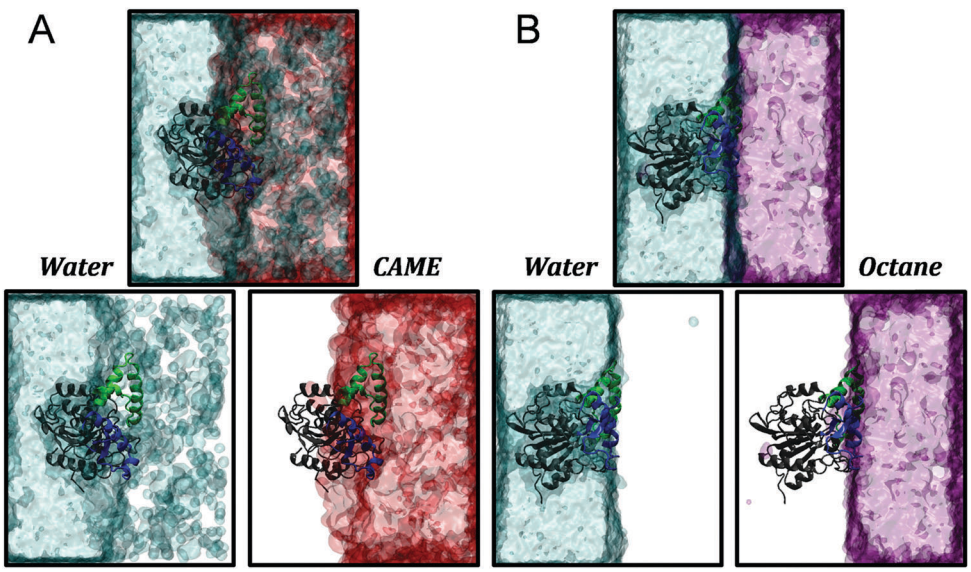

Fig. 4 Miscibility of the two phases, protein solvation, and orientation of the enzyme at the interface. (A) Water (cyan) is partially soluble in the CAME (red) phase. The interface is thus thick and rough, such that BCL is significantly solvated by both solvents. (B) The interface of water (cyan) and octane (purple) is thin and well defined, because of the immiscibility of the components. BCL interacts with the octane phase only superficially, but also exposing the catalytic cleft to the organic phase.

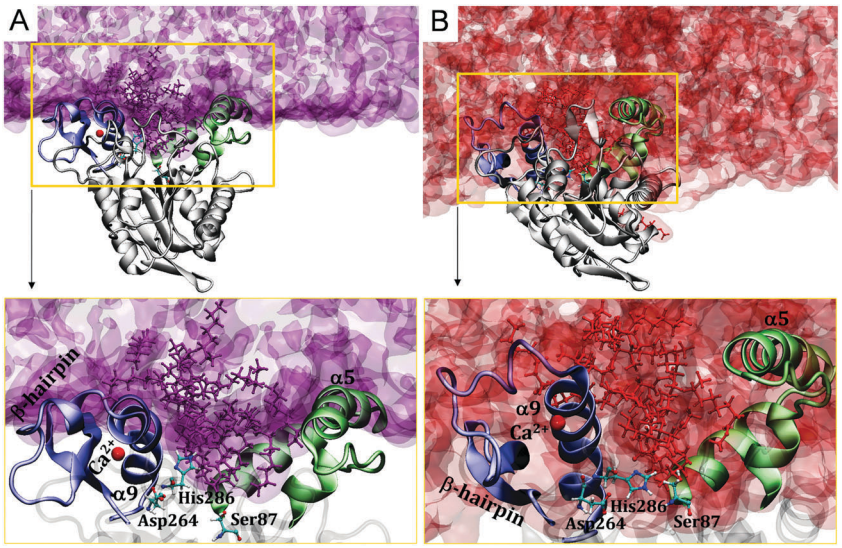

Fig. 5 The organic solvents penetrate the active-site cleft, leading to direct interactions with the catalytic triad. (A) Octane and (B) CAME.

organic solvent penetrate the active site and interact directly with the residues of the catalytic triad.

In summary, our results show that the BCL enzyme is rapidly oriented at the interfaces of water with organic solvents to expose its more hydrophilic surfaces to water and the most hydrophobic domains, and the catalytic cleft, to the organic phase. The final orientations are stable, indicating their functional relevance. The degree of hydrophobicity of the organic phase appears to be correlated with the rate of the reorientation, with every event occurring faster at the interface with octane than with CAME.

3.2 Conformational analysis of the BCL enzyme at the water/organic interfaces

The structural variability of the BCL structure at each of the interfaces was probed using structural parameters such as the gyration radius, the fraction of native contacts, and the RMSD of the protein relative to the stable structure in water, as shown in Fig. 6. The BCL structure drifts from the stable structure in water at the interfaces, but appears to achieve stable states after about 200 ns in most cases. These new stable conformations display some differences relative to the stable structure in water, including a larger radius of gyration. In one of the simulations at an octane interface a larger drift was observed.

The structural changes observed could be a sign of denaturation or of structural alterations associated with the function of the enzyme at organic interfaces.[37] We computed, therefore, the RMSD independently for each residue, to probe the regions of the protein responsible for the conformational drift observed (Fig. 7A and B). Interestingly, the regions of the protein displaying significant displacements at the interface with octane are also the regions of greater flexibility at the interface with CAME. This similarity points to a possible functional role of these fluctuations, although they might be overestimated at the octane interface. The particularly large RMSD observed in one of the octane simulations can also be explained by the same structural deviations, as shown in Fig. 7C: 80% of the protein atoms can be aligned to RMSDs smaller than 2.5 Å,[35] which reveals that the structure is overall stable. The large overall RMSD (~7 Å) is explained almost exclusively by the displacement of Helix α5, and is associated with the apperture of the catalytic pocket.

The regions of greater flexibility observed in Fig. 7 comprise the U1 and U2 domains (residues 118–166 and 215–261, respectively), which are in direct contact with the organic phase after the reorientation of the protein. In Fig. 8 we show the relative position of these domains, as measured by the distance between residues Phe142 and Gly250 (see Fig. 2B). Clearly, these domains are displaced from each other when they interact with the organic phase, particularly at the interface with octane. The distance between Phe142 and Gly250 also increases at the interface with CAME, although not to the same extent. The increased aperture of the pocket within domains U1 and U2 exposes the catalytic triad (Ser87, As264, and His286), and indicates that the conformational fluctuations observed are associated with protein activation, as previously discussed.

3.3 Aqueous–organic interfaces stabilize the open conformation of the catalytic cleft

Lipases differ from other esterases by the dependence of their activity on the substrate concentration. In particular, lipases have been shown to increase their activity upon saturation of the solution with the substrate.[38,39] Also, increased activity was also observed in the presence of organic solvents, supporting a structural role of the interfaces in their activation.[40,41] However, the BCL enzyme and other lipases are also active in aqueous solutions.[42]

The lipase might be modulated by the aperture and closure of the catalytic cleft, which appears to be favored by the interaction with the organic phases. The modulation of the exposure of the binding pocket could be kinetic or thermodynamic in nature. If the modulation is kinetic, the barrier for the transition between the closed and open states must be reduced.

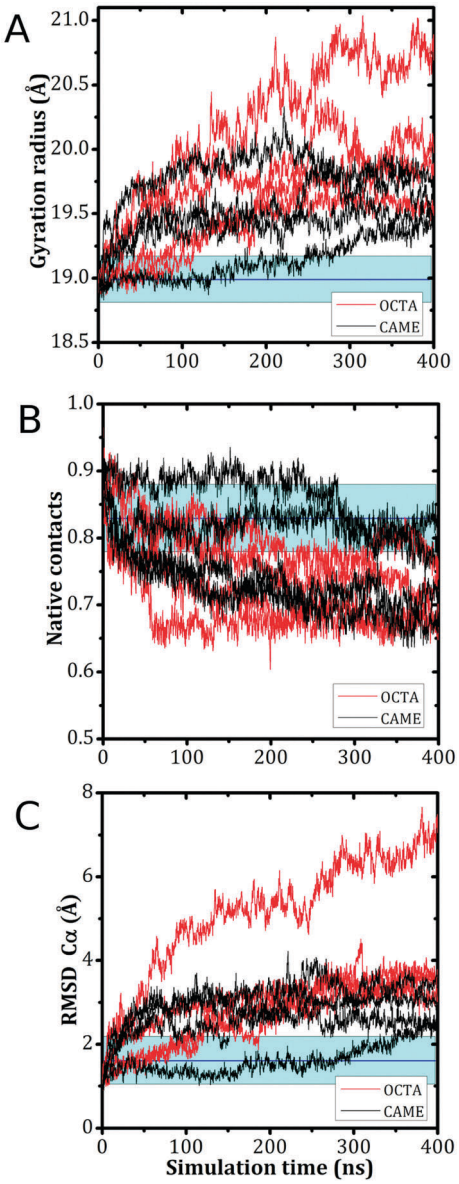

Fig. 6 Conformational analysis of BCL at the interfaces: (A) gyration radius; (B) fraction of native contacts; (C) RMSD as a function of simulation time. The blue lines and cyan shades represent the average and standard deviations of each property observed in a previous simulation of BCL in water.[36] The parameters indicate that the structures become stable after 200 ns, displaying some conformational variation relative to the most stable conformations in water. One simulation at the octane interface displayed larger structural fluctuations, which are analyzed independently in Fig. 7. In all cases, the structural changes are associated with the aperture of the catalytic pocket.

On the other hand, if the activation is thermodynamic, the interaction with the organic phase promotes the relative stabilization of the open conformation of the active site.

To probe the physicochemical mechanism of activation of the BCL enzyme at the water/organic interfaces, we have computed the free energy profiles along a reaction coordinate associated with the opening and closure of the catalytic cleft. Given that the orientation of the enzyme at the interfaces is very fast, we could use the configurations of BCL obtained from the conventional simulations described in the previous sections to initiate Adaptive Biasing Force free energy calculations of the aperture and closure of the U1 and U2 domains. Additionally, the same free energy profiles were obtained in water.

Fig. 9 shows the free energy profiles associated with the aperture of the catalytic cleft in different media. In water, the closed state (reaction coordinate $\sim$6 Å) and the open state (reaction coordinate $\sim$22 Å) have similar free energies. Therefore, the simulations indicate that BCL can be found in either the closed-inactive or open-active states with similar probabilities. Furthermore, there is a free energy barrier associated with the transition between the two states of $\sim$7 kcal mol^{-1}, implicating the transition to be a rare event at room temperature.

At the interfaces, however, there is a complete stabilization of the open state of the active site. The computed free energies of the open states are now $\sim$55 kcal mol^{-1} lower than those of the closed form. Furthermore, there is no energy barrier associated with the transition (blue and magenta lines in Fig. 9). These free energy profiles imply that at the interfaces the open state of the protein is completely dominant, and there is no kinetic barrier for the activation of the enzyme when in contact with the organic phase. Indeed, this is consistent with the observation in our simulations of the opening of the catalytic cleft in a very short time scale if compared with typical structural fluctuations of proteins. Therefore, the interaction with the organic phase, in the proper orientation, induced a fast and irreversible opening of the catalytic cleft.

From the structural perspective, we can attribute the greater stability of the open form of the enzyme to the penetration of the organic molecules in the catalytic cleft (Fig. 5). This penetration is favorable because of the hydrophobic nature of the residues of the U1 and U2 domains, and once it occurs, the volume occupied by the organic molecules obstructs the reverse mechanism, *i.e.*, the approach of helices 5 and 9.

3.4 A model for BCL activity at aqueous–organic interfaces: translation, rotation, and induced exposure of the catalytic site

The present results allow the proposal of the general mechanism of BCL activation at interfaces, with previously unknown specificity. The mechanism is shown in Fig. 10.

In water, BCL is found with equal probabilities in the closed or open forms (zero free energy difference), and there is an activation barrier associated with the transition between the two states. Since the closed form cannot bind the substrate, the activity of BCL is reduced.

In the presence of an interface with less polar media, BCL migrates to the interface and very rapidly orients itself in such a way to maximize the interaction of the hydrophobic U1 and U2 domains with the organic phase. The time-scale of this orientational phenomenon appears to be in the sub-microsecond range, thus not implying any important barrier to enzyme activation. The range of polarities sampled by octane and CAME is similar to those of the natural lipase substrates, and thus we expect that similar mechanisms and time-scales should be observed for other interfaces of biophysical relevance.

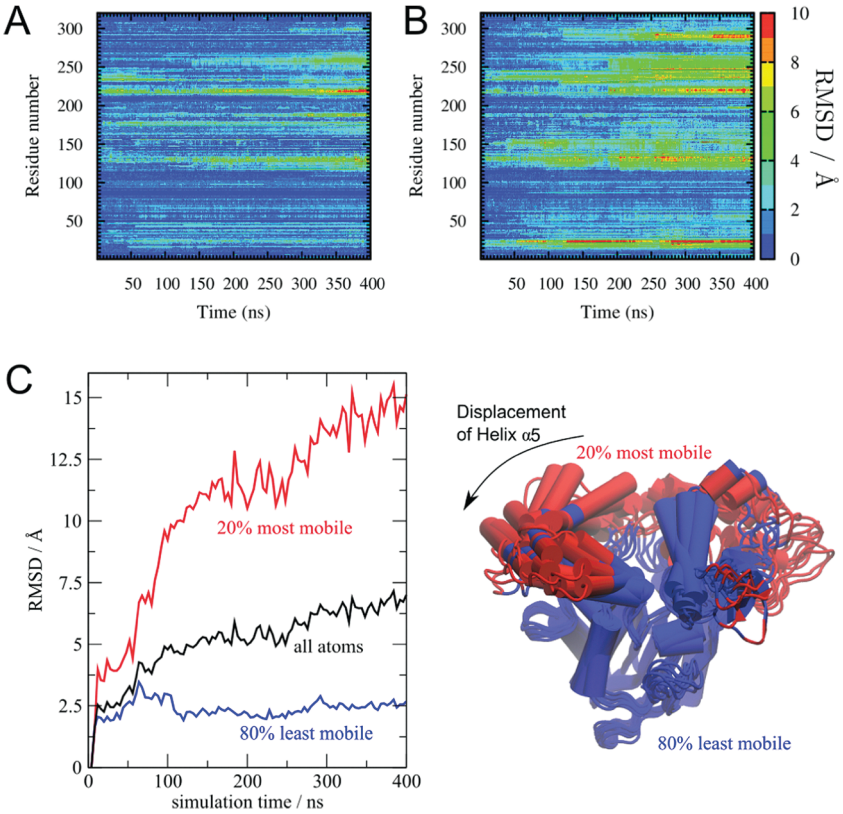

Fig. 7 Structural deviation of BCL residues as a function of time, as probed by the RMSD of the Cα atom of the residue relative to the initial structure of the simulation. (A) Interface of water and CAME. (B) Interface of water and octane. The regions displaying greater deviations are similar in both interfaces (residues 15–30; 120–160; 220–270), but the displacements observed at the octane interface are larger. (C) RMSDs of the 80% least mobile and 20% most mobile fractions of the structure, identified with the MDLovoFit package,[35] for the simulation in octane that produced the greatest deviations. Also in this case most of the structure is preserved (RMSD ~2.5 Å), and the deviations observed are associated with a large displacement of Helix α5 and the apperture of the active site.

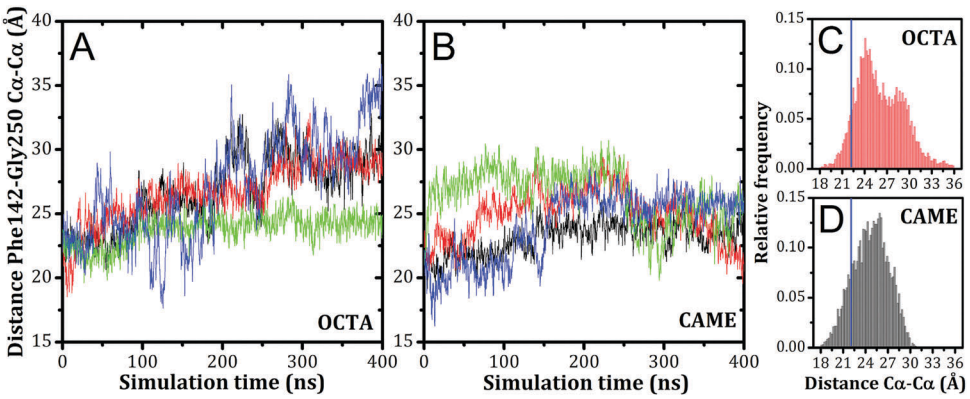

Fig. 8 Exposure of the catalytic cleft, as probed by the distance between the U1 and U2 domains of BCL following interaction with the organic phase. (A) and (B) Distances between the Cα atoms of Phe142 (from U1) and Gly250 (from U2), as a function of simulation time, indicating the increased aperture of the catalytic cleft after protein reorientation. (C) and (D) Distribution of distances at the octane and CAME interfaces, respectively. The blue vertical line indicates the distance associated with the open-form of the enzyme in water.

Finally, once the protein is properly oriented at the interface, the free energy barrier associated with the opening of the catalytic pocket is reduced, and the pocket opens allowing the penetration of molecules from the organic phase. The entrance of these molecules, usually larger than water molecules, completely stabilizes the open form of the enzyme, making the process of closure thermodynamically inaccessible at room temperature.

The facilitated access of the substrates to the catalytic pocket when the enzyme assumes the open form at the interface

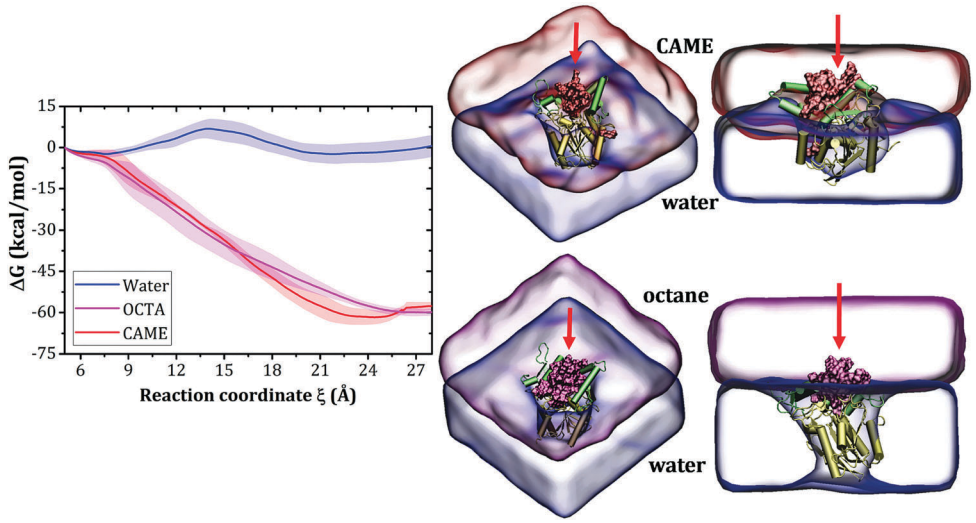

Fig. 9 Free energy profiles of the aperture of the catalytic pocket of the BCL enzyme in water and at the interfaces with octane and CAME. The lower free energy of the open forms of the enzyme at the interfaces results from the penetration of the organic molecules within domains U1 and U2, which impedes the return to the closed state. Not only does the open form of the enzyme become stable at the interfaces, but the free energy barrier associated with the transition that exists in water is eliminated. The plot represents the averages (solid lines) and standard deviations (shaded limits) of three independent ABF calculations for each system.

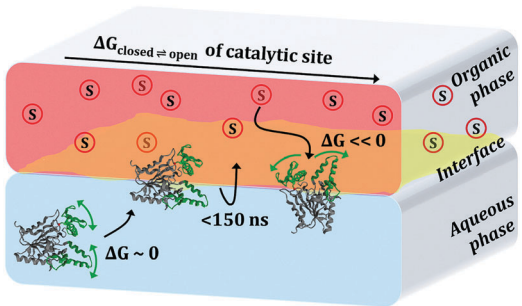

Fig. 10 Mechanism of activation of BCL in water/organic interfaces: the enzyme is partially active in water, appearing in open or closed forms with equal probability. When it reaches the interface, it rapidly reorients itself to expose the U1 and U2 domains to the organic phase. Finally, the opening of the catalytic pocket becomes highly favorable from the thermodynamic point of view, and exposes the catalytic triad to the substrate or substrate solution.

explains the augmented catalytic rates which are observed for BCL and other lipases in heterogeneous media, or in saturated substrate solutions, where the formation of agglomerates of the substrates is expected.[8,9]

4 Conclusions

In this work, we present a molecular mechanism for the activation of the *Burkholderia cepacia* lipase at aqueous/organic interfaces, using molecular dynamics simulations. We show that the enzyme displays a mechanism of reorientation at the interface which occurs in the sub-microsecond time scale. The enzyme assumes a preferential orientation at the interfaces, which maximizes the contact of the U1 and U2 domains with the less polar phase. Once properly oriented, the interaction with the organic phase facilitates the aperture of the binding pocket and, furthermore, leads to the complete stabilization of the enzyme in its open state, as demonstrated by free energy calculations. This occurs by the penetration of organic molecules into the catalytic cleft. This aperture of the binding pocket exposes the catalytic triad to the organic phase, activating the enzyme. The mechanisms observed provide a structural basis for the interfacially activated catalysis of general lipases, and might be used to inspire the design of interface-activated enzymes.

Conflicts of interest

There are no conflicts of interest to declare.

Acknowledgements

The authors would like to acknowledge the financial support of CAPES through a graduate fellowship (I. P. O.), FAPESP grants 2010/16947-9, 2013/05475-7, 2013/08293-7 and 2013/22360-9, and CNPq grant 470374/2013-6.

References

1 K. B. Zeldovich and E. I. Shakhnovich, *Annu. Rev. Phys. Chem.*, 2008, **59**, 105–127.
2 K. Jaeger, *FEMS Microbiol. Rev.*, 1994, **15**, 29–63.
3 S. Rehm, P. Trodler and J. Pleiss, *Protein Sci.*, 2010, **19**, 2122–2130.
4 B. A. Tejo, A. B. Salleh and J. Pleiss, *J. Mol. Model.*, 2004, **10**, 358–366.
5 R. L. Silveira, J. Martínez, M. S. Skaf and L. Martínez, *J. Phys. Chem. B*, 2012, **116**, 5671–5678.

6 P. R. Burney and J. Pfaendtner, *J. Phys. Chem. B*, 2013, **117**, 2662–2670.
7 M. J. Watt and G. R. Steinberg, *Biochem. J.*, 2008, **414**, 313–325.
8 P. Reis, K. Holmberg, H. Watzke, M. E. Leser and R. Miller, *Adv. Colloid Interface Sci.*, 2009, **147-148**, 237–250.
9 F. Hasan, A. A. Shah and A. Hameed, *Enzyme Microb. Technol.*, 2006, **39**, 235–251.
10 A. Aloulou, J. A. Rodriguez, S. Fernandez, D. van Oosterhout, D. Puccinelli and F. Carrière, *Biochim. Biophys. Acta*, 2006, **1761**, 995–1013.
11 R. D. Schmid and R. Verger, *Angew. Chem., Int. Ed.*, 1998, **37**, 1608–1633.
12 C. Chapus, M. Semeriva, C. Bovier-Lapierre and P. Desnuelle, *Biochemistry*, 1976, **15**, 4980–4987.
13 K. K. Kim, H. K. Song, D. H. Shin, K. Y. Hwang and S. W. Suh, *Structure*, 1997, **5**, 173–185.
14 A. Mezzetti, J. D. Schrag, C. S. Cheong and R. J. Kazlauskas, *Chem. Biol.*, 2005, **12**, 427–437.
15 P. Trodler, R. D. Schmid and J. Pleiss, *BMC Struct. Biol.*, 2009, **9**, 38.
16 S. Barbe, V. Lafaquière, D. Guieysse, P. Monsan, M. Remaud-Siméon and I. André, *Proteins*, 2009, **77**, 509–523.
17 M. R. Ganjalikhany, B. Ranjbar, A. H. Taghavi and T. T. Moghadam, *PLoS One*, 2012, **7**, e40327.
18 F. Bordes, S. Barbe, P. Escalier, L. Mourey, I. André, A. Marty and S. Tranier, *Biophys. J.*, 2010, **99**, 2225–2234.
19 J. Lee, S. W. Suh and S. Shin, *J. Biomol. Struct. Dyn.*, 2000, **18**, 297–309.
20 B. Stauch, S. J. Fisher and M. Cianci, *J. Lipid Res.*, 2015, **56**, 2348–2358.
21 J. M. Martínez and L. Martínez, *J. Comput. Chem.*, 2003, **24**, 819–825.
22 L. Martínez, R. Andrade, E. G. Birgin and J. M. Martínez, *J. Comput. Chem.*, 2009, **30**, 2157–2164.
23 L. B. Fomuso and C. C. Akoh, *Food Res. Int.*, 2002, **35**, 15–21.
24 L. Kalé, R. Skeel, M. Bhandarkar, R. Brunner, A. Gursoy, N. Krawetz, J. Phillips, A. Shinozaki, K. Varadarajan and K. Schulten, *J. Comput. Phys.*, 1999, **151**, 283–312.
25 W. Humphrey, A. Dalke and K. Schulten, *J. Mol. Graphics*, 1996, **14**, 33–38.
26 O. Guvench, S. S. Mallajosyula, E. P. Raman, E. Hatcher, K. Vanommeslaeghe, T. J. Foster, F. W. Jamison 2nd and A. D. Mackerell Jr, *J. Chem. Theory Comput.*, 2011, **7**, 3162–3180.
27 J. Huang, S. Rauscher, G. Nawrocki, T. Ran, M. Feig, B. L. de Groot, H. Grubmüller and A. D. MacKerell Jr, *Nat. Methods*, 2017, **14**, 71–73.
28 W. L. Jorgensen, J. Chandrasekhar, J. D. Madura, R. W. Impey and M. L. Klein, *J. Chem. Phys.*, 1983, **79**, 926–935.
29 K. Vanommeslaeghe and A. D. MacKerell Jr, *J. Chem. Inf. Model.*, 2012, **52**, 3144–3154.
30 K. Vanommeslaeghe, E. P. Raman and A. D. MacKerell Jr, *J. Chem. Inf. Model.*, 2012, **52**, 3155–3168.
31 A. Pohorille, C. Jarzynski and C. Chipot, *J. Phys. Chem. B*, 2010, **114**, 10235–10253.
32 J. Hénin, G. Fiorin, C. Chipot and M. L. Klein, *J. Chem. Theory Comput.*, 2010, **6**, 35–47.
33 E. Darve, D. Rodríguez-Gómez and A. Pohorille, *J. Chem. Phys.*, 2008, **128**, 144120.
34 L. Martínez, MDAnalysis, version 17.224, 2017, http://leandro.iqm.unicamp.br/mdanalysis.
35 L. Martínez, *PLoS One*, 2015, **10**, e0119264.
36 I. P. Oliveira and L. Martínez, *Phys. Chem. Chem. Phys.*, 2016, **18**, 21797–21808.
37 T. Maruyama, M. Nakajima, S. Uchikawa, H. Nabetani, S. Furusaki and M. Seki, *J. Am. Oil Chem. Soc.*, 2000, **77**, 1121–1127.
38 P. Reis, R. Miller, J. Krägel, M. Leser, V. B. Fainerman, H. Watzke and K. Holmberg, *Langmuir*, 2008, **24**, 6812–6819.
39 Z. S. Derewenda and A. M. Sharp, *Trends Biochem. Sci.*, 1993, **18**, 20–25.
40 A. Louwrier, G. J. Drtina and A. M. Klibanov, *Biotechnol. Bioeng.*, 1996, **50**, 1–5.
41 M. Kapoor and M. N. Gupta, *Process Biochem.*, 2012, **47**, 555–569.
42 A. Azizi, B. Ranjbar, K. Khajeh, T. Ghodselahi, S. Hoornam, H. Mobasheri and M. R. Ganjalikhany, *Int. J. Biol. Macromol.*, 2011, **49**, 652–656.